

MICRO-CT/MICROMECHANICS-BASED FINITE ELEMENT MODELS AND QUASI-STATIC UNLOADING TESTS DELIVER CONSISTENT VALUES FOR YOUNG'S MODULUS OF RAPID-PROTOTYPED POLYMER-CERAMIC TISSUE ENGINEERING SCAFFOLD

K. W. Luczynski¹, A. Dejaco¹, O. Lahayne¹, J. Jaroszewicz², W. Swieszkowski², C. Hellmich¹

¹Vienna University of Technology, Institute for Mechanics of Materials and Structures ²Warsaw University of Technology, Faculty of Materials Science and Engineering

Motivation

Reliable determination of elasticity from micro-CT images and micromechanics

We have recently proposed [Scheiner et al, 2009; Dejaco et al, 2012] to translate the X-ray attenuation-related grey values making up a microCT image, into voxel-specific (nano)porosities, and to resolve the microstructure (or nanostructure) within each finite element in terms of a continuum micromechanics representation [Fritsch et al. (2009)] linking (nano)porosity to material properties, as to arrive at tissue property maps across the entire imaged scaffold. These property maps turned out as reasonable input for FE simulations [Scheiner et al. (2009); Dejaco et al. (2012)]. In the present work, we extend this strategy to rapid-prototyped polymer-ceramic scaffolds [Swieszkowski et al. (2007)]. Additionally quasi-static unloading tests are performed to validate the FE-model-derived values for Young's modulus.

Materials and Methods

Micro-CT/micromechanics-based Finite Element model

A 71 volume-% macroporous tissue engineering scaffold made of poly-L-lactide (PLLA) with 10 mass-% of pseudo-spherical tri-calcium phosphate (TCP) inclusions (exhibiting diameters in the rang of several nanometers) was microCT-scanned. The corresponding stack of images was converted into regular Finite Element (FE) models consisting of around 100,000 to 1,000,000 finite elements, as described in [Dejaco et al. (2012)]. Therefore, the attenuation-related, voxel-specific grey values were converted into TCP-contents in a way similar to that described in [Dejaco et al. (2012), Scheiner et al. (2009)], and the latter, together with nanoindentation tests evaluated according to [Oliver and Pharr (1992)], entered a homogenization scheme of the Mori-Tanaka type, as to deliver voxel-specific (and hence, finite element-specific) elastic properties.

Conversion of micro-CT data into volume fractions

X-ray attenuation coefficient of PLLA-TCP composite:

$$\mu = \mu_{PLLA} f_{PLLA} + \mu_{TCP} f_{TCP}$$

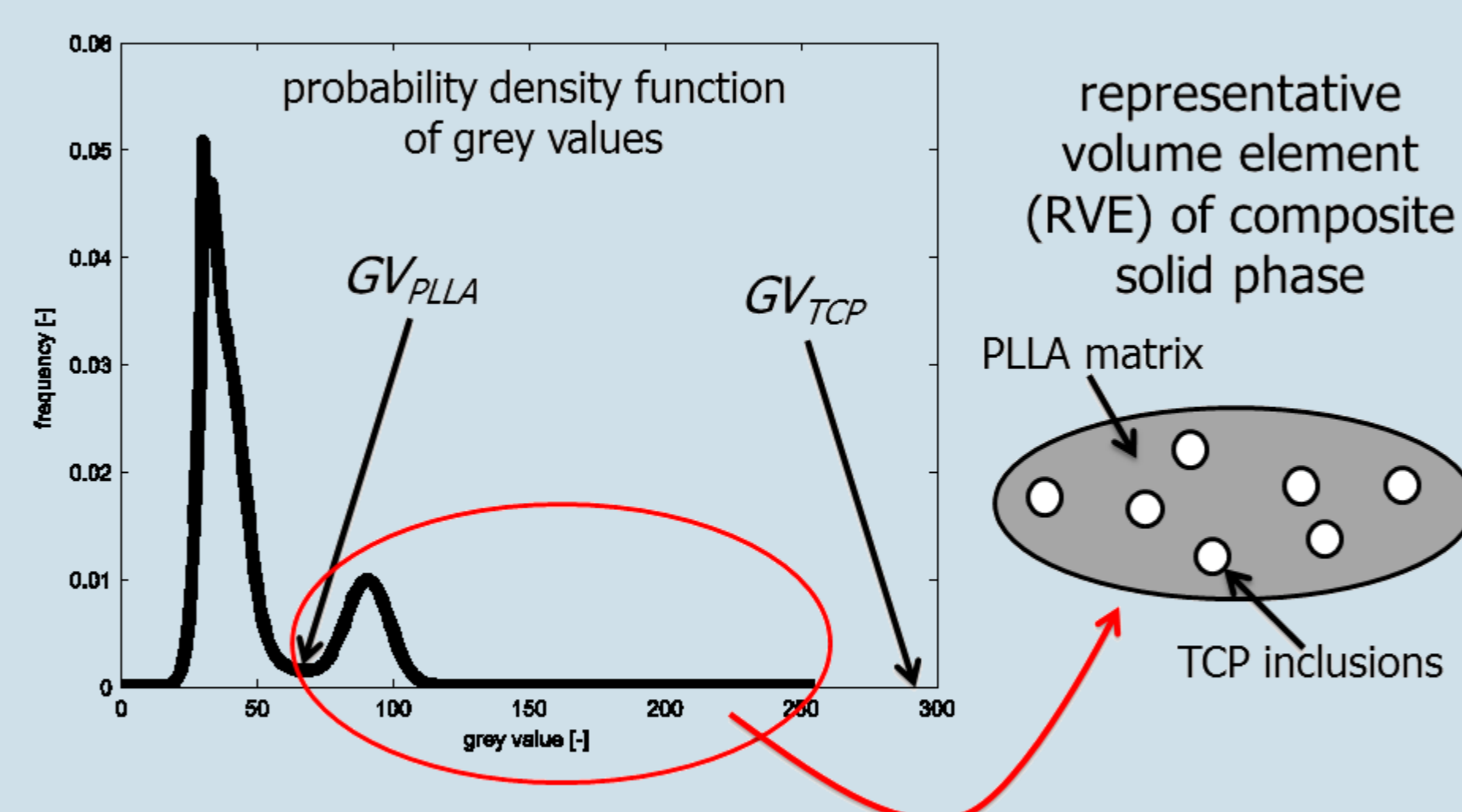
Grey value is linearly related to attenuation:

$$GV = GV_{PLLA} f_{PLLA} + GV_{TCP} f_{TCP}$$

TCP volume fraction as a function of grey value:

$$f_{TCP} = \frac{GV - GV_{PLLA}}{GV_{TCP} - GV_{PLLA}}$$

μ - X-ray attenuation coefficient (ac), μ_{PLLA} - ac of PLLA, μ_{TCP} - ac of TCP, GV - grey value, GV_{PLLA} - gv of PLLA, GV_{TCP} - gv of TCP, f_{PLLA} - PLLA volume fraction, f_{TCP} - TCP volume fraction



Homogenization of solid phase elastic properties

Effective stiffness of the solid phase as a function of grey value computed, using Mori-Tanaka scheme, from elastic properties of TCP taken from ultrasound experiments¹ ($E_{TCP}=114\text{GPa}$, $\nu_{TCP}=0.27$), and from elastic properties of PLLA stemming from nanoindentation and literature² ($E_{PLLA}=3.60\text{GPa}$, $\nu_{PLLA}=0.45$)

$$\mathbb{C}^{\text{hom}} = \left\{ (1 - f_{TCP}) \mathbb{c}_{PLLA} + f_{TCP} \mathbb{c}_{TCP} : \left[\mathbb{I} + \mathbb{P}_{\text{sph}} : (\mathbb{c}_{TCP} - \mathbb{c}_{PLLA}) \right]^{-1} \right\}$$

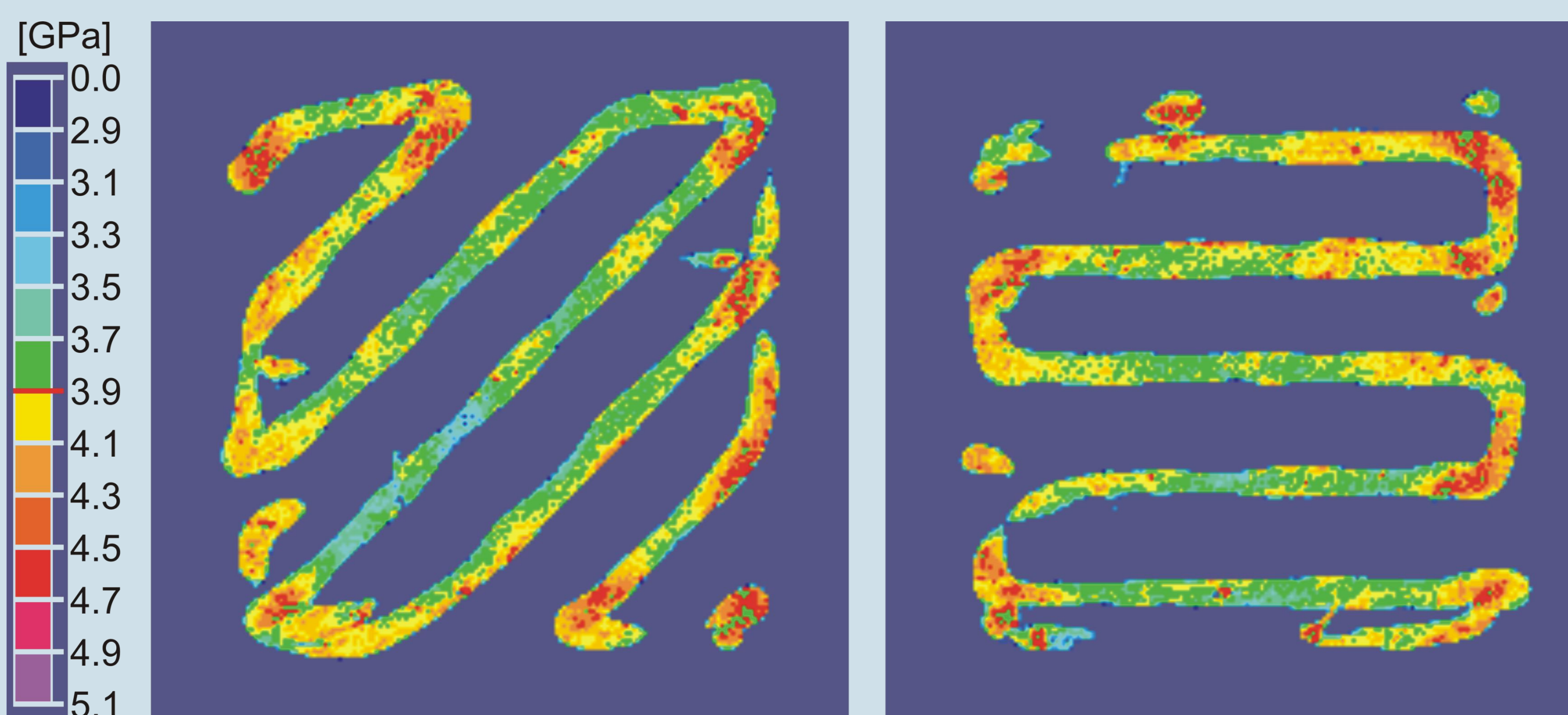
$$\left\{ (1 - f_{TCP}) \mathbb{I} + f_{TCP} \left[\mathbb{I} + \mathbb{P}_{\text{sph}} : (\mathbb{c}_{TCP} - \mathbb{c}_{PLLA}) \right]^{-1} \right\}^{-1}$$

$$\mathbb{D}^{\text{hom}} = (\mathbb{C}^{\text{hom}})^{-1} \rightarrow E^{\text{hom}} = 1 / D_{11}^{\text{hom}} \rightarrow \nu^{\text{hom}} = -E^{\text{hom}} \times D_{12}^{\text{hom}}$$

$\mathbb{C}_{PLLA} = f(E_{PLLA}, \nu_{PLLA})$ - stiffness tensor of PLLA, $\mathbb{C}_{TCP} = f(E_{TCP}, \nu_{TCP})$ - stiffness tensor of TCP, E_{PLLA} , ν_{PLLA} and E_{TCP} , ν_{TCP} respectively Young's modulus and Poisson's ratio of PLLA and TCP, \mathbb{P}_{sph} - fourth-order Hill tensor accounting for the spherical shape of the inclusions in the PLLA matrix, \mathbb{I} - fourth-order unity tensor, f_{PLLA} - PLLA volume fraction, f_{TCP} - TCP volume fraction

¹Katz and Ukraincik, J Biomech 1971, Vol 4:221-7 ²Balac et al. J Biomed Mater Res 2002, Vol. 63(6):793-799

Distribution of the Young's modulus in the scaffold's transversal cross sections



Computation of elastic engineering constants

Young's modulus

$$E_{FE} = \frac{F}{A \cdot S} = 142.9 \pm 2.7 \text{MPa}$$

F - sum of the reaction forces in the loading direction (\mathbf{e}_3)

A - area of the loaded surface

S - nominal strain in the loading direction (\mathbf{e}_3)

Poisson's ratio

$$\nu_{FE} = \frac{\nu_{13} + \nu_{23}}{2} = 0.064 \pm 0.014$$

$$\nu_{13} = -\frac{\epsilon_{11}}{\epsilon_{33}} \quad \nu_{23} = -\frac{\epsilon_{22}}{\epsilon_{33}}$$

ϵ_{11} - macro-strain in \mathbf{e}_1 (transversal) direction

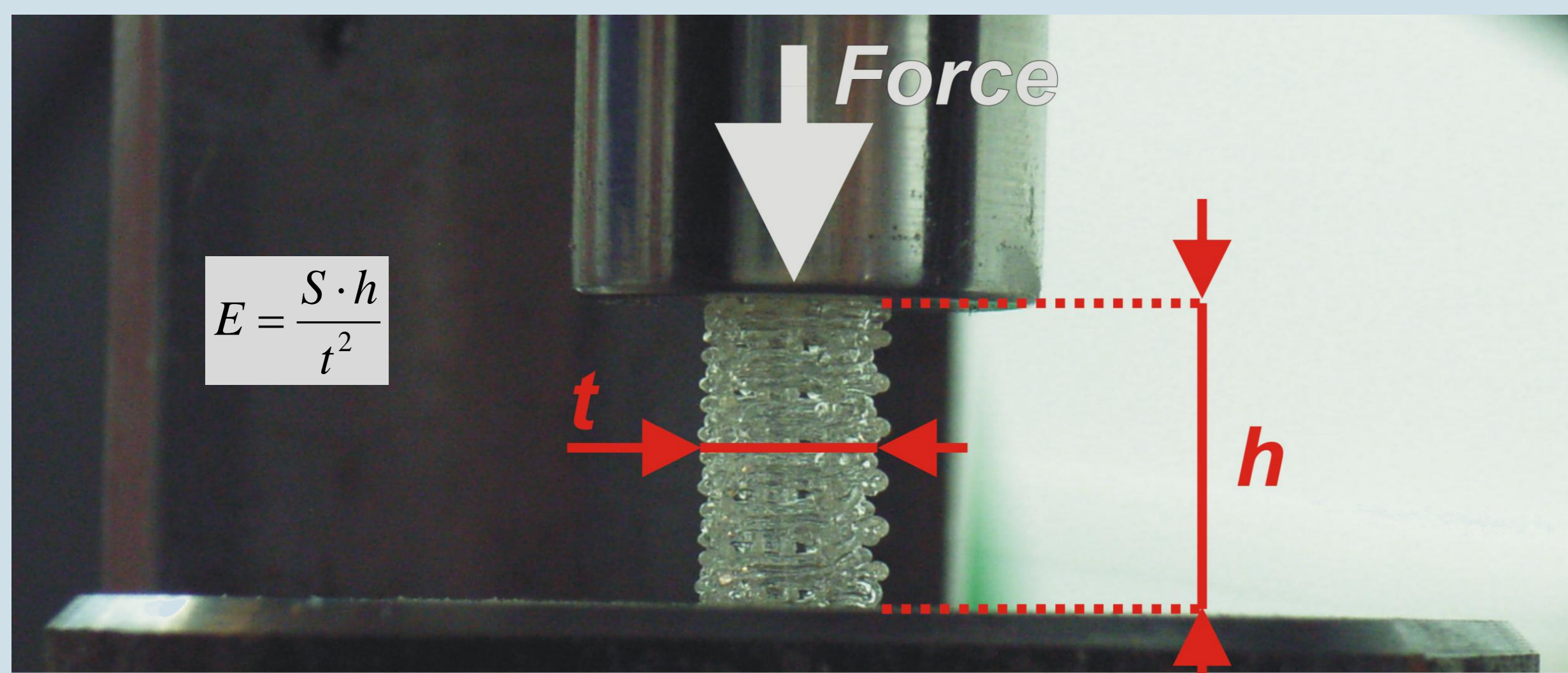
ϵ_{22} - macro-strain in \mathbf{e}_2 (transversal) direction

ϵ_{33} - macro-strain in \mathbf{e}_3 (longitudinal) direction

Quasi-static unloading tests for model validation

Force-displacement curves were recorded throughout consecutive loading-unloading cycles up to a maximum nominal strain of -0.02, -0.03, -0.04, and -0.05, with a strain rate of 0.005 s^{-1} , and the unloading regimes of these curves were evaluated. From the load maxima at the maximum applied strain levels and the corresponding displacements, the unloading curve was followed for a minimum of $50 \mu\text{m}$ along the displacement axis, and a maximum of $350 \mu\text{m}$, in $50 \mu\text{m}$ intervals. These different unloading portions were checked with respect to their linearity (indicating linear elastic properties), in terms of R^2 , the coefficient of determination between the measured forces and displacements. The slopes S of all unloading portions with $R^2 > 0.90$ are used to determine the Young's modulus of the macroporous scaffold

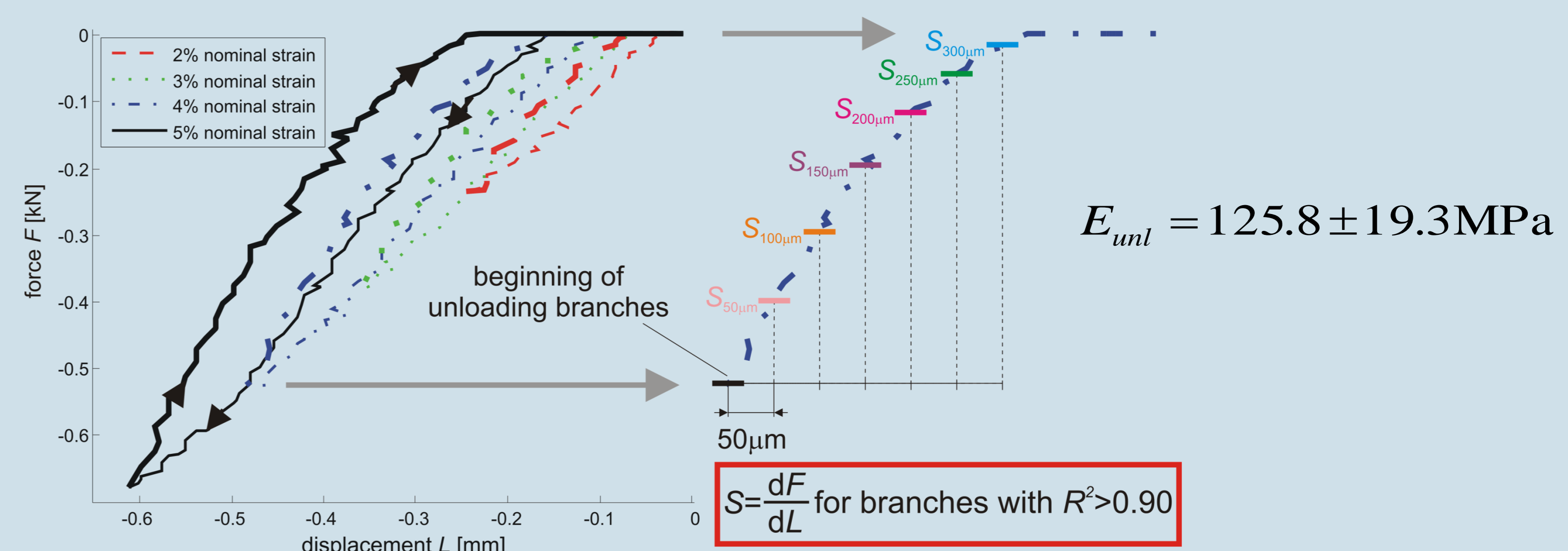
Consecutive loading-unloading cycles



computation of Young's modulus from the slope S averaged over all "linear" unloading branches

Linearity quantified in terms of coefficient of determination R^2 of a linear fit

linearity quantified in terms of coefficient of determination R^2 of a linear fit



Conclusion

FE simulations and unloading tests deliver consistent values for Young's modulus

FE simulations

$$E_{FE} = 142.9 \pm 2.7 \text{MPa}$$

H

unloading tests

$$E_{unl} = 125.8 \pm 19.3 \text{MPa}$$

H

References:

- Dejaco, A.; Komlev, V.S.; Jaroszewicz, J.; Swieszkowski, W.; Hellmich, C. (2012): Micro CT-based multiscale elasticity of double-porous (pre-cracked) hydroxyapatite granules for regenerative medicine. Journal of Biomechanics, vol. 45, pp. 1068-1075.
- Oliver, W.C.; Pharr, G.M. (2004): Measurement of hardness and elastic modulus by instrumented indentation: Advances in understanding and refinements to methodology. Journal of Materials Research, vol. 19, no. 1, pp. 3-20.
- Scheiner, S.; Sinibaldi, R.; Pichler, B.; Komlev, V.; Renghini, C.; Vitale-Brovarone, C.; Rustichelli, F.; Hellmich, C. (2009): Micromechanics of Bone Tissue-Engineering Scaffolds, Based on Resolution Error-Cleared Computer Tomography. Biomaterials, vol. 30, pp. 2411-2419.
- Swieszkowski, W.; Tuan, B.H.; Kurzydowski, K.J.; Hutmacher, D.W. (2007): Repair and regeneration of osteochondral defects in the articular joints. Biomolecular Engineering, vol. 24, no. 5, pp. 489-495.